Sensors & Transducers, Vol. 229, Issue 1, January 2019, pp. 32-38

www.sensorsportal.com

Sensors & Transducers

Published by IFSA Publishing, S. L., 2019
http://www.sensorsportal.com

Properties of Highly *c*-axis Oriented Single-crystalline ZnO Layers Grown by Sputter Epitaxy for Hydrogen Gas and UV Sensors

Ki Ando, Toshiya Kumei, A.-I. Mizuno, Hiroyuki Shinoda and Nobuki Mutsukura
Tokyo Denki University, School of Engineering,
5 Senjyu-Asahi-cho, Adachi-ku, Tokyo, 120-8551, Japan
Tel.: + 81-3-5284-5433, fax: + 81-3-5284-5691

Received: 30 November 2018 /Accepted: 31 December 2018 /Published: 31 January 2019

Abstract: We have previously developed ultra-high vacuum RF magnetron sputtering systems. They can produce high-quality single-crystalline compound semiconductor layers without grain boundaries on sapphire substrates. We aim to utilize these semiconductor layers in high-sensitivity sensor devices used for detecting leakage hydrogen gas (H_2) from storage facilities and for early finding UV irradiation from accidental hydrogen flames. This study demonstrates the sensitivity of our single-crystalline zinc oxide (ZnO) layers to detect H_2 and UV irradiation. In the result, the H_2 sensor showed sufficient sensitivity to detect up to 5 ppm of H_2. Moreover, the UV sensor could detect UV irradiation of 0.01 μW/cm^2 at wavelength of 360 nm. Although as-grown single-crystalline ZnO layers is used without employing any sensitivity-enhancement techniques, these sensors could achieve the sensitivity equal to that of commercial devices. Thus, we considered that our single-crystalline ZnO layers using sensitivity-enhancement techniques could yield ultra-high sensitivity devises.

Keywords: Hydrogen gas sensor, UV sensor, Zinc oxide (ZnO), Sputter epitaxy, Single-crystalline layer.

1. Introduction

Sputtering is a common inexpencive method for depositting various materials as thin films; however, these films do not have high crystallinity. We have previously developed ultra-high vacuum RF magnetron sputtering systems that could achieve ultimate pressures of 10^{-8} Pa and ultra-high substrate temperatures up to 1200 °C [1]. These systems can produce high-quality single-crystalline compound semiconductor layers, such as gallium nitride (GaN) and zinc oxide (ZnO) on sapphire substrates [2-3]. High crystalline orientation of these layers was revealed via X-ray diffraction (XRD) measurement and any grain boundaries and cracks on the layers were not found as far as observation by scanning electron microscopy (SEM). Our next purpose is utilize these high-quality semiconductor layers in high-sensitive sensors. To this end, we have discussed the utility of using our single-crystalline ZnO layers for hydrogen gas (H_2) and UV sensors at international conferences [4].

Detection of leakage H_2 from its storage facilities and early finding accidental hydrogen flames are becoming important along with developing the hydrogen energy system [5-8]. Therefore, high-sensitivity of H_2 and flame sensors are further required in the future. Metal oxide (MOX) semiconductor materials, such as ZnO and tin oxide (SnO_2), are highly sensitive to various gases and they are often

used in gas sensors [9-10]. Hydrogen flame is invisible, but it radiates UV light. UV light detection is suitable for early finding hydrogen flames, because UV light detection has advantages for immediacy and small disturbance over heat source detection [7-8]. Several MOX semiconductor materials have bandgaps greater than 3 eV; therefore, they can be used for high-sensitivity UV sensors without requiring visible light-blocking filters unlike silicon semiconductor-based UV sensors [11].

Most resistive MOX semiconductor gas and UV sensors employ nanostructure layers in the form of nanorods, nanowires, or grain layers. Several studies have applied thin-film and crystalline layers to gas and UV sensors [12-13]; however, these layers exhibit a poly-crystalline structure. Although single-crystalline MOX semiconductors possess ideal electrical properties to be used in sensors, their high production cost and difficult fabrication has limited their use in H_2 and UV sensors.

This study demonstrates the sensitivity of our single-crystalline ZnO layers to detect H_2 and UV irradiation. Additionally, our aim is not only developing high-sensitivity sensors but also suggesting a hybrid sensor device for both H_2 and UV detection which is manufactured on one ZnO layer for detecting hydrogen accidents effectively.

2. Materials and Methods

2.1. Growth Process of ZnO Layers

Single-crystalline ZnO layers were grown on sapphire [α-Al_2O_3(0001)] substrates using our developed ultra-high vacuum RF magnetron sputtering system, as shown in Fig. 1.

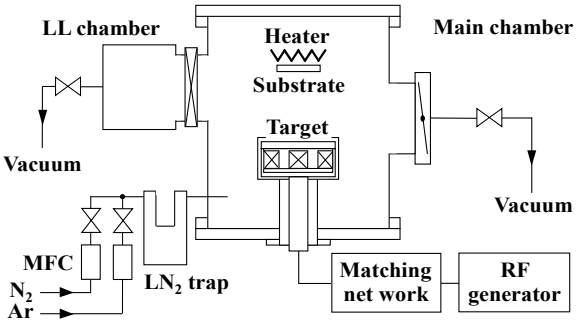

Fig. 1. Schematic diagram of the sputtering system.

A 5-N grade ZnO sintered compact was used as a sputtering target. Prior to deposition, the main chamber was evacuated to less than 1.5×10^{-6} Pa. 6-N grade argon gas (Ar) purified by a liquid N_2 trap was used as the sputtering gas. Ar flow rate was regulated 5 sccm, and Ar pressure was set to 2 Pa. The 13.56 MHz RF power input was regulated 100 W. When ZnO layers were deposited on the substrate for application in UV sensors, 4 % of 6-N grade nitrogen gas (N_2) was mixed with the sputtering gas to compensate by acceptors for any electron carriers present in ZnO layer defects. Substrate temperature while depositing was set to 550 °C when the layer was used as a H_2 sensor and to 780 °C when the layer was used as a UV sensor. Deposition time was 30 min, and resulting layer thickness was 860 nm (H_2 sensor) and 570 nm (UV sensor).

2.2. Properties of ZnO Layers

Electrical conduction properties of these layers were n-type, and electrical properties, which were measured by the van der Pauw method, are shown in Table 1. Preliminary experiments showed that a lower carrier density of ZnO layers provided better H_2 and UV sensitivity; however, some deposition parameters described above differed depending on the purpose of use of the produced layer. The surface morphology of layers used as H_2 sensors were controlled to an ultrafine, not completely flat structure. Alternatively, when layers were used as UV sensors, only low electron density was considered over other parameters.

Table 1. Electrical properties of ZnO layers.

	Electron density	Electron mobility	Resistivity
H_2 sensor	4.3×10^{16} cm^{-3}	5.6 $cm^2/V \cdot s$	25 Ω·cm
UV sensor	3.3×10^{16} cm^{-3}	3.9 $cm^2/V \cdot s$	49 Ω·cm

The crystalline quality of ZnO layers used for sensors was evaluated via XRD measurements, and the results of the layer used as the H_2 sensor are shown in Fig. 2. The $2\theta/\omega$ scan mode showed a single and narrow peak for the ZnO (0002) face, indicating that the ZnO layer had high *c*-axis orientation. Using the ω scan mode, FWHM of the ZnO (0002) peak was 1140 arcsec; this narrow peak suggested that the layer had high uniformity of *c*-axis tilt-angle. The relation of peaks between ZnO and Al_2O_3 in φ scan mode revealed that the ZnO layer had an epitaxial relation with the sapphire substrate. In cases wherein the layer was used as the UV sensor, $2\theta/\omega$ scan mode showed the same result as Fig. 2(a), FWHM of the ZnO (0002) peak in ω scan mode was 540 arcsec, and the result of its φ scan mode showed the same relation of Fig. 2(c).

Fig. 3 shows the SEM images of the ZnO layers, which shows that they had a flat surface and fine structures. Grain boundaries were not present in the layers as far as we observed by SEM. Additionally, root mean square surface roughness of the layers used as H_2 and UV sensors reached to 1.6 and 3.3 nm, respectively. These results imply that these were single-crystalline ZnO layers.

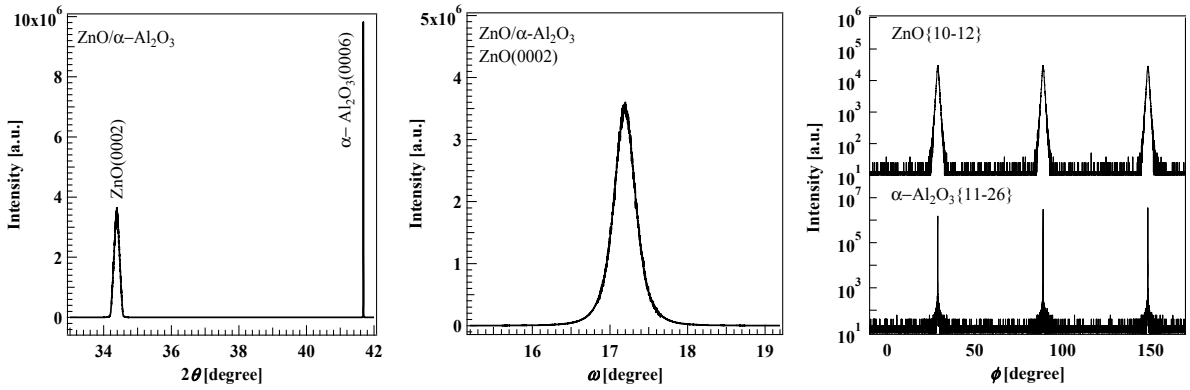

(a) $2\theta/\omega$ scan mode (b) ω scan mode (c) φ scan mode

Fig. 2. XRD spectrum of the ZnO layer used as the H_2 sensor.

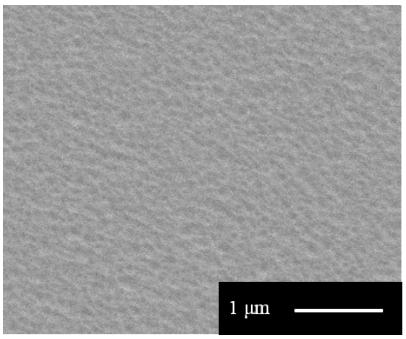

(a) Used as H_2 sensor

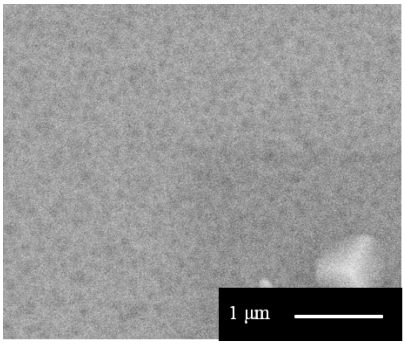

(b) Used as UV sensor

Fig. 3. The surface SEM images of the ZnO layers.

2.3. Sensor Device Structures and Evaluation Systems

Both H_2 sensor and UV sensor demonstrated in this paper were resistive devices. Sensor device structures are shown in Fig 4. Gold and titanium (Au/Ti) electrodes were deposited on the ZnO surface in parallel. We confirmed that ohmic contact was established between these electrodes and the ZnO layers. In the H_2 sensor, nickel (Ni) wires were bonded on each Au electrode using silver (Ag) paste. In the UV sensor, needles of phosphor bronze were placed on each Au electrode to have electric contact. Both sensors had sensor area of 3×7 mm.

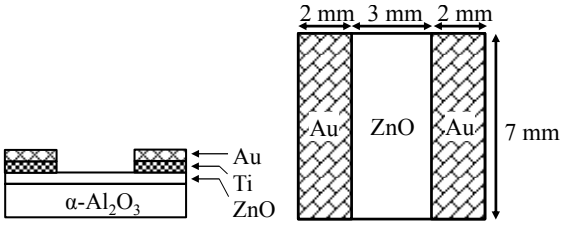

(a) Cross-sectional view (b) Top view

Fig. 4. Schematic of the sensors.

Fig. 5 schematizes the evaluation systems of the H_2 and UV sensors. In evaluations of both sensors, 5 V bias voltage was applied between each electrode; resistance changes in the sensor was observed via sensor current, which passed through the ZnO layer, measured using a digital multimeter (DMM).

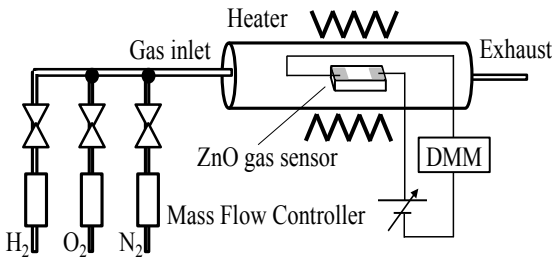

(a) Used for the evaluation of H_2 sensor

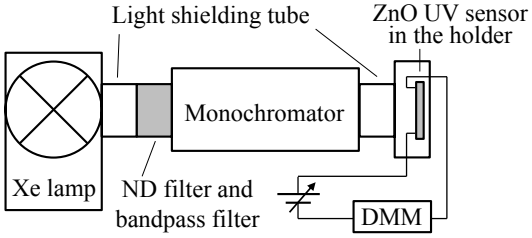

(b) Used for the evaluation of UV sensor

Fig. 5. Schematic of the evaluation systems.

Heating is required to adsorb gas onto the sensor surface for operating resistive MOX semiconductor gas sensors [14-15]. Therefore, H_2 sensor was heated to 400 °C in a tubular electric furnace. The sensor was placed in a fused glass tube; both ends were capped using silicon rubber caps containing a gas inlet and outlet tube. A standard gas mixture of 6-N grade 20 % O_2 and 80 % N_2 was used, which is hereafter referred to as "air". For obtaining sensor response to H_2, 6-N grade H_2 was mixed with O_2 and N_2; H_2 was predetermined concentration, O_2 was constant 20 %, and N_2 was used as balance gas. This mixed gas was described as "H_2 gas" and distinguish it by denoting its H_2 concentration. These mixed gas pressures were atmospheric pressure, and flow rates were regulated to 50 sccm in total.

For evaluating the UV sensor, a xenon (Xe) lamp was used as a light source for irradiating and exciting the ZnO layer. Irradiation power was reduced by neutral density (ND) filters, and desired wavelength was selected using bandpass filters and a monochromator. This experiment was performed in a dark room at room temperature.

3. Results

3.1. Response of the H_2 Sensor

When the H_2 sensor is heated in air condition, resistance of the sensor is increased by binding of electrons caused by the adsorption of O_2 onto the sensor surface. Conversely, when H_2 gas flows into the sensor, the resistance is decreased by released and supplied electrons, resulting from the adsorption of H_2 onto the sensor surface. These behaviors are affected by the work temperature of the sensor, and a higher resistance ratio between air and H_2 gas conditions imparts higher sensitivity to H_2.

Therefore, we investigated the dependence of sensor resistance on work temperature in air and 1 % H_2 gas condition. We evaluated these sensor current after varying the work temperature and waiting until the current reached a steady state. In air condition, the current significantly decreased at 300 °C work temperature or more, as shown in Fig. 6. In 1 % H_2 gas condition, the current decreased at 450 °C work temperature or more due to thermal desorption of H_2. We observed similar work-temperature dependency in other ZnO layers; therefore, 400 °C was considered as the suitable work temperature for our ZnO H_2 sensors.

Prior to investigating H_2 sensitivity, the sensor was heated at 400 °C in air condition until the sensor current reached a steady state. We defined this steady-state current value as base current I_{air}. In this case, I_{air} was 7.1 nA. When H_2 gas flowed into the sensor, the sensor current increased, as shown in Fig. 7. H_2 gas conditions was kept for 10 min, and current at the end of the period was evaluated as H_2 gas response I_{H2}. The responsivity ratio R_r was calculated as the ratio between I_{air} and I_{H2} using Equation (1).

$$R_r = (I_{H2} - I_{air})/I_{air} \quad (1)$$

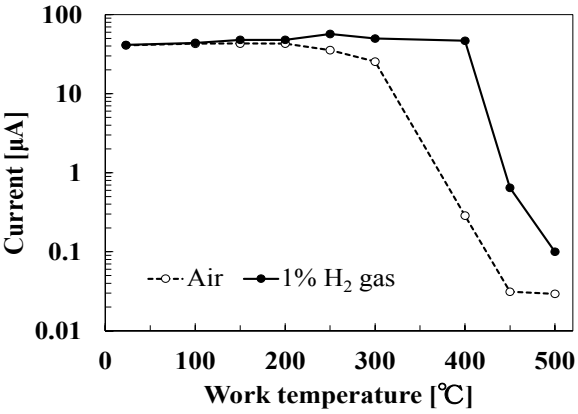

Fig. 6. Dependence of sensor resistance on work temperature in each gas condition.

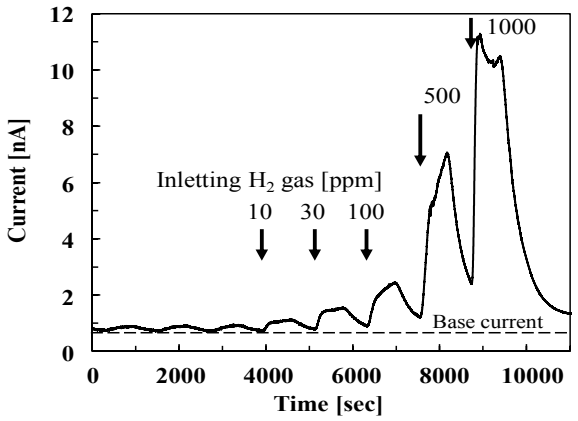

Fig. 7. Response of the H_2 sensor to change in gas condition.

The sensor showed significant response to low H_2 gas conditions less than 10 ppm, as shown in Fig. 8. R_r was calculated as 0.3 at 10 ppm H_2 gas condition, as shown in Fig. 9. R_r at 7 ppm was approximately equal to that at 6 ppm or less. Responsivity R was defined using H_2 gas concentration C_{H2} using Equation (2).

$$R = (I_{H2} - I_{air})/C_{H2} \quad (2)$$

R of this sensor was around 0.25 nA/ppm under low H_2 gas conditions. Therefore, we considered that the limit of detection of this sensor was 5 ppm H_2, but the limit of resolution was 10 ppm H_2.

Large surface areas for adsorbing gases and formation of depletion layers at bottleneck structure of grain boundaries are effective for enabling dynamic resistance changes of MOX semiconductor gas sensors [14-15]. Although our ZnO layer did not have bottleneck structures, the H_2 sensor could detect up to 5 ppm H_2. We considered that the ultrafine structures of the ZnO layer surface provided sufficient surface areas for gas-molecule adsorption, and a depletion layer was present from the ZnO surface to thickness

direction [16-17]. Moreover, due to the ZnO layer having higher crystallinity than that in conventional sensors, it has lower electron density and higher electron mobility. Therefore, it was suggested that these characteristics led to less parasitic resistance, thereby increasing the response to gas [18].

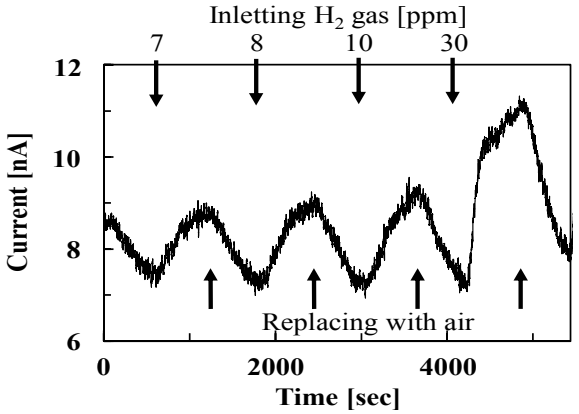

Fig. 8. Response of the H_2 sensor in low H_2 gas condition.

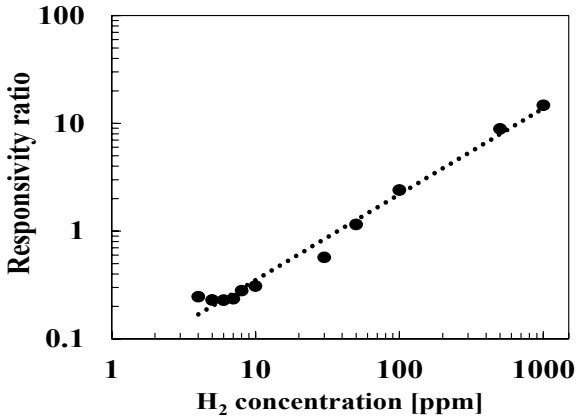

Fig. 9. Responsivity ratio (R_r) of the H_2 sensor to H_2 concentration.

3.2. Response of the UV Sensor

Fig. 10 shows the transmittance of the ZnO layer used as the UV sensor. Visible light and infrared irradiation passed through it and UV irradiation less than wavelength of 360 nm was absorbed completely. This cutoff wavelength matched well 3.37 eV bandgap energy of ZnO. Additionally, these sharp cutoff characteristics demonstrated that this ZnO layer had high crystallinity and few defects.

The resistance of the UV sensor decreases at irradiating light due to the photoexcited carrier and increases after obstructing the light. Prior to evaluating photo-response, we placed the sensor in dark until the sensor current reached steady state. We denoted this steady-state current value as the dark current. We then irradiated light to the sensor for 10 min and measured the current value at the end of the period, defining this value as the photocurrent.

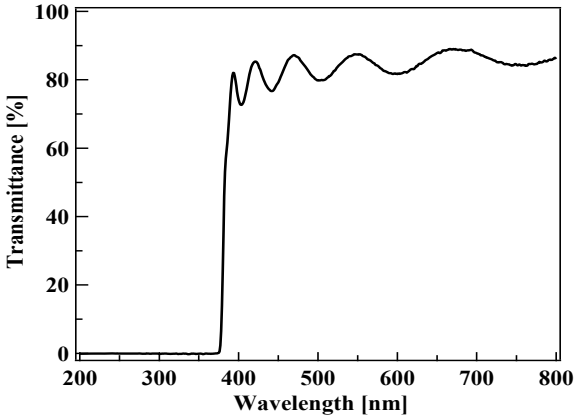

Fig. 10. Transmittance of the ZnO layer used as the UV sensor.

Fig. 11 shows wavelength dependence of the photocurrent of the UV sensor. Its radiant emittance was unified to 42 μW/cm^2. When irradiated by visible or infrared light, the sensor current was only slightly greater than the dark current. In contrast, the sensor current significantly increased by UV irradiation of wavelength less than 380 nm. This result correlated with the transmittance characteristics shown in Fig. 10. The maximum sensor response was to wavelength of 360 nm.

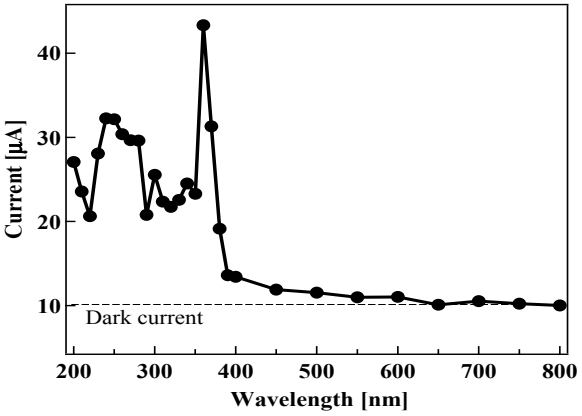

Fig. 11. Wavelength dependence of the photocurrent of the UV sensor.

Fig. 12 shows the photo response to wavelength of 360 nm and to radiant emittance of 0.013 to 42 μW/cm^2. The sensor current increased at commencement of UV irradiation. From this response, the responsivity ratio R_r was calculated using dark current I_{dark}, photo current I_{photo} via Equation (3).

$$R_r = (I_{photo} - I_{dark})/I_{dark} \quad (3)$$

R_r was 0.043 at radiant emittance of 0.013 μW/cm^2, as shown in Fig. 13, where I_{dark} was 10.67 μA. In addition, responsivity of this sensor R_s and normalized

responsivity R_n were defined using power of radiant emittance P and sensor area A, as Equation (4) and Equation (5).

$$R_s = (I_{photo} - I_{dark}) / P, \quad (4)$$

$$R_n = (I_{photo} - I_{dark}) / PA \quad (5)$$

R_s and R_n were 35 μA/μW·cm^{-2} and 170 μA/μW at radiant emittance of 0.013 μW/cm^2, respectively. From this result, we considered that the UV sensor had limits of detection and resolution of 0.01 μW/cm^2 UV irradiation at 360 nm.

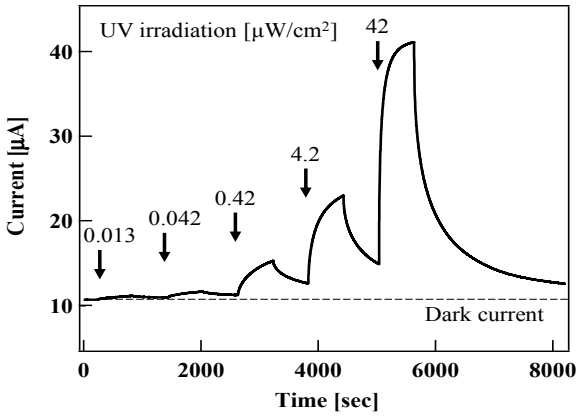

Fig. 12. Response of the UV sensor to wavelength of 360 nm.

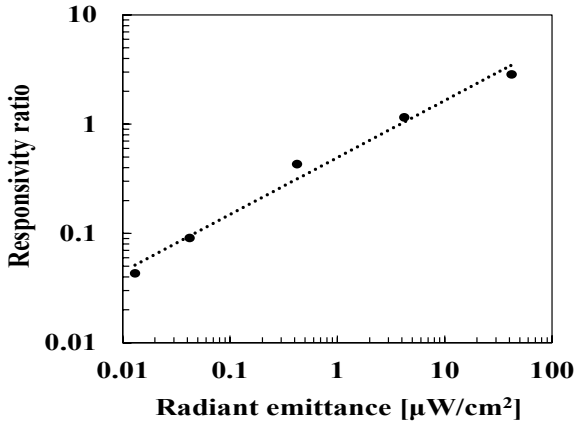

Fig. 13. Responsivity ratio (R_r) of the ZnO layer to UV irradiation.

Finally, we determined the R_r of various ZnO layers having different electron densities; these relations are depicted in Fig. 14. A lower electron density in the ZnO layer led to a greater R_r. R_r also correlated with electron mobility in ZnO layers ranged from 3.0 to 51 cm^2/V·s; however, R_r was more closely dependent on electron density. We conclude that the high-crystallinity ZnO layers have the advantage of low electron density due to being minimal defects, and minimal defects may also prevent the trapping of photoexcited carriers. Therefore, the ZnO layer containing low electron density significantly led to low dark current and an enhanced current ratio between dark and photoexcited conditions.

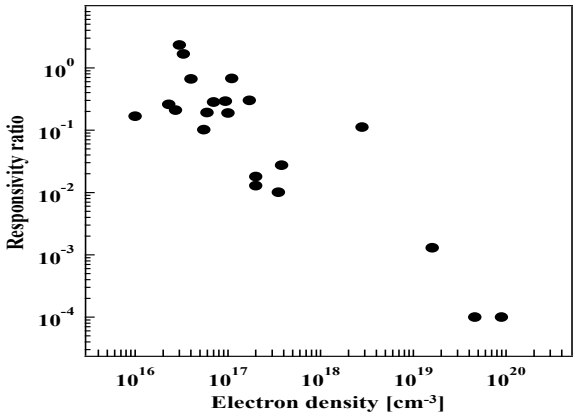

Fig. 14. Dependence of responsivity ratio (R_r) on electron density of ZnO layers.

4. Conclusions

This study demonstrated the high sensitivity of H_2 and UV sensors utilized highly *c*-axis oriented single-crystalline ZnO layers grown by using our developed sputtering system. These ZnO layers had ultrafine structures on the flat surface without grain boundaries. Their electrical properties were superior to those of conventional resistive MOX semiconductor gas and UV sensors. Furthermore, the sensitivity of our sensors was equal or superior to that of reported devices: the H_2 sensor could detect H_2 up to 5 ppm, and the UV sensor could detect UV irradiation up to 0.01 μW/cm^2.

Our ZnO sensors showed several advantages due to high crystallinity. Although we used as-grown single-crystalline ZnO layers without employing sensitivity-enhancement techniques, the sensitivity of our sensors was comparable with that of commercial devices. Thus, our ZnO sensors developed using sensitivity-enhancement techniques should achieve even greater sensitivities.

Additionally, our ZnO layers did not show mutually exclusive requirements for their respective detection capabilities of H_2 and UV. Therefore, we intend to develop a hybrid sensor device manufactured on one ZnO layer which is capable of detecting both leakage H_2 gas and accidental hydrogen flames.

Acknowledgements

A part of this work was conducted at Advanced Characterization Nanotechnology Platform of the University of Tokyo, supported by "Nanotechnology Platform" of the Ministry of Education, Culture, Sports, Science and Technology (MEXT).

A part of this work was supported by LIXIL JS Foundation, No. 17-84.

The authors also would like to thank members of our laboratory for helping our experiments: Mr. Kohei Ogura operated the sputtering system, and he analyzed properties of ZnO layers. Mr. Tomoki Shinta established the evaluation system of UV sensors, and he investigated the responses of UV sensors. Ms. Asuka Fujikawa proposed great ideas for developing H_2 gas sensors, and she performed measurements of the sensors.

References

[1]. N. Mutsukura, H. Shinoda, Highly *c*-axis oriented AlN layers grown on *c*-plane sapphire substrates by radio-frequency sputter epitaxy at 1080 °C, *Thin Solid Films*, Vol. 520, Issue 13, 2012, pp. 4237-4241.

[2]. H. Shinoda, N. Mutsukura, Preparation and properties of GaN:Al layers grown by radio frequency magnetron sputter epitaxy, *Vacuum*, Vol. 138, 2017, pp. 87-92.

[3]. H. Shinoda, N. Mutsukura, Structural properties of GaN layers grown on Al_2O_3 (0001) and GaN/Al_2O_3 template by reactive radio-frequency magnetron sputter epitaxy, *Vacuum*, Vol. 125, 2016, pp. 133-140.

[4]. K. Ando, T. Kumei, A. Watanabe, A. Mizuno, H. Shinoda, N. Mutsukura, Application of Highly c-axis Oriented Single-Crystalline ZnO Layers Grown by Sputter Epitaxy to Hydrogen Gas Sensor and UV Sensor, in *Proceedings of the 4th International Conference on Sensors and Electronic Instrumentation Advances (SEIA' 2018)*, Amsterdam, The Netherlands, 2018, pp. 102-106.

[5]. S. Phanichphant, Semiconductor Metal Oxides as Hydrogen Gas Sensors, *Procedia Engineering*, Vol. 87, 2014, pp. 795-802.

[6]. T. Hubert, L. Boon-Brett, V. Palmisano, M. A. Bader, Developments in gas sensor technology for hydrogen safety, *International Journal of Hydrogen Energy*, Vol. 39, Issue 35, 2014, pp. 20474-20483.

[7]. T. Oshima, T. Okuno, N. Arai, N. Suzuki, H. Hino, S. Fujita, Flame Detection by a β-Ga_2O_3-Based Sensor, *Japanese Journal of Applied Physics*. Vol. 48, No. 1R, 2009.

[8]. M. Razeghi, Short-Wavelength Solar-Blind Detectors – Status, Prospects, and Markets, *Proceedings of the IEEE*, Vol. 90, Issue 6, June 2002, pp. 1006-1014.

[9]. A. Dey, Semiconductor metal oxide gas sensors: A review, *Materials Science & Engineering B*. Vol. 229, 2018, pp. 206-217.

[10]. G. Korotcenkov, B. K. Cho, Metal oxide composites in conductometric gas sensors: Achievements and challenges, *Sensors and Actuators B: Chemical*, Vol. 244, 2017, pp. 182-210.

[11]. Z. Alaie, S. Mohammad Nejad, M. H. Yousefi, Recent advances in ultraviolet photodetectors, Materials *Science in Semiconductor Processing*, Vol. 29, 2015, pp. 16-55.

[12]. K. Zhanga, Z. Yanga, M. Wanga, M. Caoa, Z. Suna, J. Shao, Low temperature annealed ZnO film UV photodetector with fast photoresponse, *Sensors and Actuators A*, Vol. 253, 2017, pp. 173-180.

[13]. P. S. Shewalea, Y. S. Yua, UV photodetection properties of pulsed laser deposited Cu-doped ZnO thin film, *Ceramics International*, Vol. 43, Issue 3, 2017, pp. 4175-4182.

[14]. N. Barsan, M. Schweizer-Berberich, W. Göpel, Fundamental and practical aspects in the design of nanoscaled SnO_2 gas sensors: a status report, *Fresenius' Journal of Analytical Chemistry*, Vol. 365, Issue 4, 1999, pp. 287-304.

[15]. C. Wang, L. Yin, L. Zhang, D. Xiang, R. Gao, Metal Oxide Gas Sensors: Sensitivity and Influencing Factors, *Sensors*, Vol. 10, Issue 3, 2010, pp. 2088-2106.

[16]. W. Göpel, K. D. Schierbaum, SnO_2 sensors: current status and future prospects, *Sensors and Actuators B: Chemical*, Vol. 26, Issue 1-3, 1995, pp. 1-12.

[17]. N. Barsan, D. Koziej, U. Weimar, Metal oxide-based gas sensor research: How to?, *Sensors and Actuators B: Chemical*, Vol. 121, Issue 1, 2007, pp. 18-35.

[18]. H. Kim, J. Lee, Highly sensitive and selective gas sensors using p-type oxide semiconductors: Overview, *Sensors and Actuators B: Chemical*, Vol. 192, 2014, pp. 607-627.